Czech Academy of Sciences

Thesis of the Doctor of Sciences Dissertation in
CHEMICAL SCIENCES

Active sites in zeolite catalysts. A DFT approach

Committee for the defense of doctoral dissertations in
the field of PHYSICAL CHEMISTRY

Štěpán Sklenák

J. Heyrovský Institute of Physical Chemistry of the
Czech Academy of Sciences

Prague 2023

Contents

Résumé

In this Thesis I summarize my research carried out using DFT approaches deeply intertwined with experiments. My research contributed to the solutions of several key problems in the area of heterogenous catalysis over industrially important zeolitic crystalline aluminosilicate catalysts. The broad coupling of the theoretical parts of the studies with the corresponding experimental counterparts required using (i) realistic computational models based on the available experimental data, (ii) the computational methodology adequate for the studied system, (iii) proper sampling of the configuration space if necessary, and (iv) comparison of the theoretical results with the experimental ones and eventual improvement of the computational model and the method used if needed. This successful integration of the theoretical and experimental contributions allowed relevant theoretical predictions for very complex industrially relevant catalytic systems.

I performed my research regarding (i) the optimization of the acid and redox zeolite–catalyst functionality via the control of the organization of Al atoms in the zeolite framework, (ii) the elucidation of the structure–function relationship of active sites in zeolite catalysts, (iii) the design of a new type of enzyme–function mimicking active sites activating small molecules as N_2O and especially O_2, and (iv) the development of highly active catalysts for the selective oxidation of methane by dioxygen. The knowledge of (i) the organization of Al atoms in the framework of Si–rich zeolites and (ii) the local structure of cationic sites for bare divalent transition metal cations in these zeolites enabled our predictions of a possible formation of distant binuclear cationic sites and their ability to split dioxygen using only DFT modeling.

The Al organization in zeolites is a key property controlling the performance of the zeolite catalyst by determining the local arrangement of the active site, its nature, and the position in the zeolite microporous channel system. Learning the Al organization of a zeolite is needed to evaluate its potential for individual catalytic reactions. Nevertheless, the exclusively experimental approach using multi–nuclear solid–state NMR cannot

be applied on complex structures of industrially relevant zeolites. Our development of the methodology for the calculations of ^{27}Al NMR parameters of framework Al atoms and ^{7}Li as well as ^{23}Na NMR parameters of extra–framework Li^{+} and Na^{+}, respectively, cations coordinated to AlO$_4^{-}$ tetrahedra allowed the interpretation of the experimental data. These theoretical and experimental results permitted the development of the methodology for the analysis of the location of the framework negative charge in complex zeolite structures. These results represent the complex analysis of the Al organization in ferrierite and a significant step ahead in understanding the Al siting in the second most important zeolite in catalysis – ZSM–5.

Electron–pair acceptor Al Lewis sites in zeolite catalysts represent active sites for a number of acid–base reactions. Using ^{27}Al solid state NMR experiments interpreted via DFT culations we suggested and confirmed the structure of framework Al Lewis sites in the beta zeolite which is the key Lewis acid catalyst applied in industry. We also proposed a plausible mechanism of the formation of the Al Lewis sites in the beta zeolite.

Employing the obtained knowledge regarding the Al distribution, theoretical modeling allowed the determination of the local structure of cationic sites for bare divalent transition metal cations at the atomic level, which cannot be obtained by diffraction method experiments, that is essential for understanding redox reactions over metallozeolite catalysts.

DFT calculations of the reactivity of two cooperating transition metal cations were essential for the discovery of a new type of the active sites capable of the M(II) to M(IV) redox cycle able to activate small low reactive molecules. The activation of dioxygen exhibits extraordinary importance. Furthermore, the cleavage of dioxygen occurs by a new mechanism – dioxygen splitting at low temperature. The pairs of the distant α–oxygen atoms formed by dioxygen splitting are exceptionally active and are able to oxidize methane at low temperatures. These achievements represent a real breakthrough in oxidation catalysis over metallozeolites.

1. Introduction

Catalysis is generally associated with underpinning approximately 30% of gross domestic product in European economies.[1] Catalysis is involved at some point in the processing of over 80% of all manufactured products.[1] Zeolites compose the most important group of heterogenous industrial catalysts. The need of (i) the transformation of the chemical production to a sustainable one and (ii) the decarbonization and transfer to new substrates requires the development of a new generation of heterogeneous catalysts, especially zeolite–based ones. Zeolites are very widely applied due to their (i) enormous tunability allowing a high activity and selectivity, (ii) mechanical and chemical stability, and (iii) excellent transport properties and accessibility of reaction centers. The design of advanced catalytic systems exhibiting high activity and selectivity and meeting requirements of industrial applications represents a complex process that cannot be performed without the detailed knowledge of the properties of the catalysts.

Zeolites are crystalline microporous aluminosilicates $[Si_{n-m}Al_mO_{2n}]^{m-}$ made of corner sharing TO_4 tetrahedra (T = Si and Al^-; Si in SiO_4 and Al^- in AlO_4^- are isoelectronic). There are two types of zeolite atoms – framework ones and extra–framework species. The former form the framework of a zeolite while the latter which are positively charged coordinate to framework O atoms of AlO_4^- tetrahedra to compensate the negative charge introduced by framework Al^- atoms. A typical feature of many silicon–rich zeolites is a high number of crystallographically distinguishable T (i.e., tetrahedral) sites. Since the protons, cations, and metal–oxo species (i.e., positively charged extra–framework species) bind to O atoms of AlO_4^- tetrahedra, the crystallographic position of aluminum in the zeolite framework governs the location of the active sites, which in turn affects the catalytic activity and selectivity.[2]

The organization[3] of Al atoms in the framework of Si–rich zeolite catalysts is a key property.[3-6] The Al organization[3] includes (i) the Al siting (i.e., which different crystallographically distinguishable framework T sites are

occupied by various types of Al atoms),[7] (ii) the Al distribution (the distribution of framework aluminum atoms among various types of Al atoms),[3] and (iii) the location of framework Al atoms of interest in the channel system of the zeolite.[8] The positively charged active species balance the negative charge of AlO_4^- tetrahedra, and therefore, the organization of Al atoms in the zeolite framework controls the formation and properties of active sites in the zeolite.[4-5, 8-11] The Al siting determines the position of the active sites in the zeolite framework while the Al distribution controls the concentration and stability of mono and divalent cations and metal–oxo species.[3-5, 12-21] In addition, for monovalent cationic species including protons, the Al distribution also controls the distance between the active sites and thus a possibility of their cooperation.[22-23] Obtaining insights into the Al organization is of crucial importance for the development of new better catalysts as catalytic studies showed that zeolites of the same chemical composition but different Al organization could possessed different catalytic properties.[4-6, 8, 24-25] Thus, the potential of a zeolite for individual catalytic reactions cannot be evaluated without the knowledge of the Al organization in the framework.

Diffraction techniques cannot distinguish between Al and Si atoms in the zeolite framework, and therefore, do not allow direct identification of the Al siting in zeolites.[2, 26-27] The Al siting of Si–rich zeolites with several crystallographically distinguishable T sites had not been known before 2007. We developed the new bare framework model[2, 26-30] which includes neither water molecules nor explicitly counter cations and used it in our DFT calculations in tandem with ^{27}Al (3Q) and ^{29}Si MAS NMR spectroscopy and determined for the first time (i) the partial Al siting in a set of ZSM–5 zeolites[2, 26, 29] and (ii) the full Al siting in a set of ferrierite.[27] The interpretation of the ^{27}Al (3Q) NMR spectra would not have been possible without our DFT calculations. Our developed methodology to determine the Al siting was subsequently used by others.[31-32]

In addition, we showed for the first time that monovalent cations (e.g., Li^+ and Na^+) in dehydrated zeolite

frameworks could be used as probes of the Al siting.[17, 21] However, even in this case diffraction methods could not be employed to study Li^+ and Na^+ centers **in Si–rich zeolites** because of a large number of possible cationic sites and a low or no occupancy by the cation of these sites due to a low content of the cation in the zeolite.[7, 17, 21] Therefore, we developed a new methodology using high–resolution multinuclear ^7Li and ^{23}Na solid–state NMR spectroscopy coupled with DFT calculations and showed that this methodology represents a powerful tool to identify the corresponding siting.[17, 21]

Li^+ cations (monitored by ^7Li MAS NMR spectroscopy coupled with DFT computations) employed as probes of the Al siting can serve as a complementary method to ^{27}Al (3Q) MAS NMR spectroscopy. Li^+ cations are very likely the most useful probes among monovalent cations because they are small and strongly coordinate to one or two framework oxygen atoms of AlO_4^-.[17] Na^+ cations monitored by ^{23}Na (3Q) MAS NMR in tandem with DFT calculations can determine the ring forming the Na^+ site but not which T site is occupied by Al in that ring.[21]

Besides Brønsted acid SiOHAl groups formed by protons compensating tetrahedral AlO_4^-, also electron–pair acceptor Al Lewis sites are often present in zeolite catalysts.[33-35] The Al Lewis sites were suggested to correspond to Al centers tricoordinated to the zeolite framework.[34, 36-37] However, this type of Al has resisted detection by ^{27}Al MAS NMR till our investigation.[38] Our subsequent solid–state NMR and DFT study[39] for the first time (i) showed that the electron–pair acceptor of the Al framework (Al_{FR}) Lewis sites corresponded to an Al_{TRI} atom tricoordinated to the zeolite framework which adsorbed a water molecule and (ii) proposed a plausible mechanism of the formation of (Al_{FR}) Lewis sites in the beta zeolite.

In contrast to the Al organization, the siting and location of bare divalent cations M(II) in the rings and the channel systems, respectively, were known[9-11] for a number of Si–rich catalysts analyzed by experimental methods – UV–vis combined with FTIR spectroscopy of Co(II) cations.

9

However, obtaining the local structure and stability of these sites would have required the knowledge of the Al siting and even with this it could have been elucidated only by DFT calculations. Therefore, we developed a new procedure to obtain the local structure and stability of cationic sites formed by bare divalent cations accommodated in 6–rings and 8–rings. We discovered that periodic DFT calculations including molecular dynamics simulations or other similar global optimization techniques must have been used.[3, 15, 18, 20, 40-45] We showed that the accommodation of bare divalent cations in rings forming cationic sites could have led to significant rearrangements of the local structures of the zeolite framework, and therefore, the precise local structure of sites binding a divalent cation could not have been derived from results of X–ray crystallography and neutron diffraction crystallography experiments, but could have been inferred from theoretical calculations.[3, 15, 18, 20, 40-45] The calculated structure of the M(II) sites represents a starting point for the investigation of the performance of the cations in catalysis. Moreover, in zeolites with highly complex structures, the empiric interpretation of the spectroscopic experiments is not sufficient even for the analysis of the Me(II) siting in the ring and the channel.[20] Our newly developed methodology was applied for the analysis of industrially important zeolite catalysts for the first time.[3, 15, 18, 20, 40-45]

Distant binuclear cationic sites were firstly identified using theoretical modeling in the context of the study of the N_2O decomposition over the Fe(II) cation exchanged ferrierite, the beta zeolite, and ZSM–5 (i.e., Fe–ferrierite, Fe–beta, and Fe–ZSM–5, respectively).[46] We devised that the presence of the active sites formed by the distant binuclear Fe(II) centers explained the exceptional activity of Fe–ferrierite in comparison with the Fe–beta and Fe–ZSM–5 catalysts.[40] The first chemical step of the N_2O decomposition is the formation of the α–oxygen species[40-41] [i.e., $(Fe(IV){=}O)^{2+}$] which exhibits unique oxidation properties reflected in an outstanding activity in the oxidation of methane to methanol at room temperature.[41, 47-51]

Furthermore, we predicted for the first time employing periodic DFT calculations and subsequently confirmed experimentally that the ferrierite zeolite exchanged with other transition metal cations able of the M(II) to M(IV) redox cycle could be employed for the preparation of the α–oxygen species [i.e., $(M(IV)=O)^{2+}$] using N_2O.[41]

Moreover, we firstly predicted using the power of periodic DFT calculations that these distant binuclear cationic sites were able to split dioxygen to yield pairs of the distant α–oxygen species.[43] Subsequently, experiments were performed at room temperature and the theoretical prediction of a cleavage of dioxygen to give a pair of the distant α–oxygen atoms was confirmed experimentally and thus splitting dioxygen was discovered.[43] A pair of the formed distant α–oxygen species [i.e., $(Fe(IV)=O)^{2+}$] features exclusive oxidation properties manifested in an exceptional activity in the oxidation of methane to methanol at room temperature.[43] Theoretical modeling further clearly showed that this breakthrough[52] in the activation of dioxygen was not limited exclusively to Fe(II) cations but the ability of dioxygen splitting represented a general property of the distant binuclear M(II) centers capable of the M(II) to M(IV) redox cycle with the Me...Me distance of ca 7.4 Å stabilized in M(II)–ferrierite.[44] These findings were afterward verified experimentally.[53] In addition, our computational study revealed that the distant binuclear Fe(II) sites with suitable parameters accommodated in various zeolites can split dioxygen to form a pair of the distant α–oxygen species as well.[45] This outcome is most likely true also for other M(II) cations capable of the M(II) to M(IV) redox cycle. Therefore, the ability to cleave dioxygen represents a general property of the distant binuclear M(II) centers stabilized in aluminosilicate matrices, and thus suggesting the possibility of developing M–zeolite–based systems for the dioxygen activation for direct oxidations using various zeolite matrices.[45] Afterward, our DFT study revealed that the proximity of the other $(Fe(IV)=O)^{2+}$ site in the confined reaction space of the zeolite cavity could dramatically change

the behavior of both the cooperating α–oxygen atoms and the reaction mechanism over $(Fe(IV){=}O)^{2+}$ sites of a pair of the distant α–oxygen atoms could differ from that over isolated $(Fe(IV){=}O)^{2+}$ sites.[54]

This Thesis describes the developments and results regarding the theoretical part of the determination of the Al organization including the key development of the bare framework model which allowed the simplification of the computational model to calculate reliable NMR parameters for the zeolites of interest. This permitted the achievement of the determination of (i) the partial siting of isolated single Al atoms in a set of ZSM–5 zeolites and (ii) the full siting of both isolated single Al atoms and Al–O–(Si–O)$_2$–Al sequences in a set of ferrierite zeolites including the ferrierite sample used to prepare the distant binuclear cationic sites. The Thesis further reveals the local structure and dynamics of cationic sites for bare divalent cations in various zeolites. All the mentioned knowledge enabled our identification of the distant binuclear Fe(II) sites using theoretical modeling. These centers are responsible for the facile N_2O decomposition in the Fe–ferrierite catalyst. Employing the power of periodic DFT calculations we predicted that these distant binuclear cationic sites could split dioxygen at room temperature to yield pairs of the distant α–oxygen species able to oxidize methane to methanol at room temperature. Based on this theoretical prediction, we discovered a cleavage of dioxygen over distant binuclear cationic sites employing Mössbauer and FTIR experiments and stoichiometric reaction tests. This achievement represents a breakthrough in oxidation catalysis.[52] The obtained knowledge regarding the Al organization of the zeolites of interest and concerning the local structure of M(II) cationic sites was a necessary condition to discover splitting dioxygen on distant binuclear Fe(II) cationic sites, and subsequently, to prepare the α–oxygen atoms (using N_2O or O_2) on Fe(II) and M(II) cations other than Fe(II).

2. Computational methods and programs

Atomistic simulations of catalytic reactions over solid catalysts are a challenge to modern computational chemistry. To model a catalytic process, the computational method used should correctly evaluate: (a) the interactions between the reactants, transition states, intermediates, products on the one hand and the catalyst on the other hand; (b) the thermodynamics and kinetics of the catalytic reaction steps to provide reasonable values for reaction energies and barriers; (c) the method should also be able to correctly describe the structural complexity of the catalyst.

A twofold approach is needed to computationally model a catalyst. On the one hand, the theoretical model used must include all the important features (e.g., the active sites) as well as the structural complexity of the catalyst. On the other hand, the theoretical method employed has to be able to correctly describe all the important interactions. Since the computer time and resource demand grow polynomially with the size of the model, there is always a tradeoff between the size and complexity of the catalyst model on the one hand, and the theoretical method used on the other hand.

Reliable predictions of the NMR parameters (i.e., NMR shielding tensors,[55] and moreover for quadrupolar nuclei, also nuclear quadrupolar coupling constants[55] (C_Q) and asymmetry parameters[55] (η)) of zeolite framework atoms or extra–framework cations require both (i) accurate predictions of the local structure of the atoms of interest (e.g., framework AlO_4^- and SiO_4 tetrahedra as well as extra–framework cations and their corresponding cationic sites) since the calculated NMR parameters are very sensitive to small changes of the local structure and (ii) reliable calculations of the corresponding NMR parameters from the optimized structures.

In order to realistically model the structure, reactivity, and properties of zeolites as well as to computationally investigate the catalytic activity of zeolite catalysts, a computational model of these structurally

complex systems has to be built based on experimental structural data. The best structures are those obtained by X–ray crystallography and neutron diffraction crystallography at good resolution. The computational models have to include a large number of atoms.

3. Al organization: computational models and methods
3.1. Development of the bare zeolite framework model – model of fully hydrated zeolites

High–resolution ^{27}Al MAS NMR spectra of zeolites can be successfully measured only for fully hydrated matrices due to the strong quadrupolar interaction of the aluminum atoms in dehydrated zeolite.[2, 19, 26-27, 29-30] Therefore, the NMR parameters characterizing the Al atoms and their environments in the zeolite frameworks can be measured only for zeolites containing counter cations or H_3O^+ and water molecules. Due to an enormous number of possible configurations, isotropic chemical shift calculations including the hydration of zeolite and the solvated counter cation would require extensive sampling over isotropic chemical shifts calculated quantum mechanically for the individual configurations and structures.[2, 26-27, 29-30] To avoid this huge computational problem, we developed a simple model of the complex structure of a hydrated zeolite. We employ a bare charged framework with a single Al atom in a unit cell to describe the local geometry around the Al nucleus of isolated single Al atoms. Similarly, two Al atoms are used to characterize the local geometry about the two Al nuclei of $Al-O-(Si-O)_n-Al$ (n = 1, 2, and 3) sequences. Each Al atom bears a formal charge of -1. This is a realistic model because of the reasons as follows: in completely hydrated zeolites, the fully solvated counter cation is located close to the center of the cavity/channel and does not directly interact with the AlO_4^- tetrahedra as evidenced by a number of XRD studies of hydrated zeolites.[56] Our study showed that the effect of the hydrated counter cation on the local geometry of the AlO_4^- tetrahedra in hydrated Si–rich zeolites and thus on the ^{27}Al isotropic chemical shift was negligible.[2, 26-27] The

development of the bare framework model which includes neither water molecules nor explicitly counter cations represents the crucial step which permitted the computations of reliable local structures and NMR parameters for the zeolites of interest due to the simplification of the computational model. In addition, the bare framework model can be employed to calculate the local geometry of framework SiO_4 tetrahedra and ^{29}Si chemical shifts of framework Si atoms of both hydrated and dehydrated zeolites.[30, 57] The bare framework model was used to determine the partial siting of isolated single Al atoms in a set of ZSM–5 zeolites,[2, 26] Al siting in the ZSM–22 and Theta–1 zeolites,[28] and the full siting of both isolated single Al atoms and Al–O–$(Si–O)_2$–Al sequences in a set of ferrierite zeolites.[27] Furthermore, this model was utilized to establish the effects of Al/Si and Ge/Si substitutions and silanol nests on the local geometry of Al and Si framework sites and the ^{27}Al and ^{29}Si, respectively, NMR parameters in the SSZ–13 zeolite[30] and the Ge and Al containing zeotype of the zeolite beta polymorph C (BEC) structure,[57] respectively. Moreover, the effects of the presence of Al–O–Si–O–Al and Al–O–$(Si–O)_2$–Al sequences in the ZSM–5 zeolite framework on the local geometry of AlO_4^- tetrahedra and the ^{27}Al NMR parameters were investigated employing the bare zeolite framework model.[29] In addition, the same model was utilized to determine the siting of close unpaired Al atoms in the SSZ–13 zeolite.[3]

3.2. Models of dehydrated zeolites

Computational models of dehydrated zeolites are composed of framework atoms and extra–framework cations. The tetrahedral framework Al atoms are fully charge balanced. These models were utilized to investigate:

1) The quadrupolar interaction of ^{27}Al nuclei in dehydrated zeolites.[19]
2) The Li^+ and Na^+ siting in Li–ferrierite[17] and Na–ferrierite,[21] respectively, matrices.

3) The structure and formation of Al Lewis sites.[38-39]

4) The structure and stability of cationic sites formed by bare divalent cations.[3, 15, 18, 20, 40-45, 54, 58-59]

4. Al organization: results

4.1. Determination of the partial siting of isolated single Al atoms in ZSM–5[2, 26]

We demonstrated investigating a set of eighteen differently synthesized ZSM–5 zeolites featuring predominantly isolated single Al atoms that a combined experimental (^{27}Al (3Q) MAS NMR) and theoretical (QM–Pot employing the bare framework model) approach represented a powerful tool for the determination of the local geometry of framework AlO_4^- tetrahedra, the prediction of ^{27}Al isotropic chemical shifts in hydrated zeolites, and the identification of Al siting in the framework of Si–rich zeolites. We determined that the occupation of the framework T–sites by Al and the concentration of Al in these T–sites were neither random nor controlled by a simple rule. They both depend on the conditions of the zeolite synthesis. Our study provided experimental evidence for the occupation of at least 12 out of 24 distinguishable framework T–sites by Al atoms in Si–rich ZSM–5.

4.2. Effect of Al–O–Si–O–Al and Al–O–(Si–O)$_2$–Al pairs in the ZSM–5 zeolite framework on the ^{27}Al NMR spectra[29]

The effect of the presence of Al–O–Si–O–Al and Al–O–(Si–O)$_2$–Al sequences in the ZSM–5 zeolite framework on the local geometry of AlO_4^- tetrahedra and the ^{27}Al NMR parameters was investigated employing ^{27}Al 3Q MAS NMR spectroscopy and QM–Pot calculations. The Al–O–(Si–O)$_2$–Al chains form the α and β cationic sites for bare divalent cations. Our calculations revealed that the presence of an Al atom as a next–nearest (Al–O–Si–O–Al) and next–next–nearest (Al–O–(Si–O)$_2$–Al) neighbor could significantly

16

affect both the local geometry of AlO_4^- tetrahedra as well as ^{27}Al NMR isotropic chemical shift (up to 4 ppm).

There is no systematic contribution of Al in Al–O–Si–O–Al or Al–O–(Si–O)$_2$–Al chains to the ^{27}Al isotropic chemical shift, and not even the direction can be predicted without explicit DFT calculations. Our investigation showed that the method to determine the Al siting in ZSM–5 used in our study[2, 26] can be employed only for ZSM–5 samples having a low or negligible concentration of Al–O–Si–O–Al and Al–O–(Si–O)$_2$–Al sequences in the zeolite matrix, otherwise ^{27}Al (3Q) MAS NMR spectroscopy cannot be used to even identify the number of framework T sites occupied by Al.

4.3. The location of isolated single Al atoms and Al−O−(Si−O)$_2$−Al sequences of interest in the channel system of the zeolites[8]

The location can be either in the channels or at the channel intersections. Our study on ZSM–5 zeolites shows that zeolites prepared using exclusively TPA$^+$ as a structure–directing agent (i.e., in the absence of Na$^+$ cations) led to 55–90% of Al atoms located at the channel intersection, regardless the presence or absence of Al pairs in the zeolite framework. The presence of Na$^+$ cations in the synthesis gel did not modify the Al location at the channel intersection (55–95% of Al atoms) and led only to changes in i) the distribution of framework Al atoms between Al pairs (decrease) and single isolated Al atoms (increase), and ii) the siting of Al in distinguishable framework tetrahedral sites.

4.4. Determination of the siting of isolated single Al atoms in ZSM–22 and Theta[28]

Our QM/MM calculations in tandem with the already published ^{27}Al 3Q MAS NMR experimental data on the Si–rich ZSM–22 and Theta–1 zeolites of the TON structure showed that Al atoms could be located in 6 framework T positions because the two eightfold sites (T1 and T2) split into four fourfold T sites after an Al/Si substitution.

4.5. Complete determination of the siting of Al atoms in Si–rich zeolites of the ferrierite structure[27]

Employing a set of five differently synthesized ferrierite zeolites we developed a multistep method allowing determination of the complete Al distribution in Si–rich zeolites with fewer crystallographically distinguishable framework T sites independent of the presence of Al–O–Si–O–Al or Al–O–(Si–O)$_2$–Al sequences in their frameworks. This approach combined multispectroscopic experiments with periodic DFT calculations.

The complete Al siting in the three ferrierite samples with only isolated single Al atoms and two ferrierites with Al–O–(Si–O)$_2$–Al sequences was determined (Figure 1).
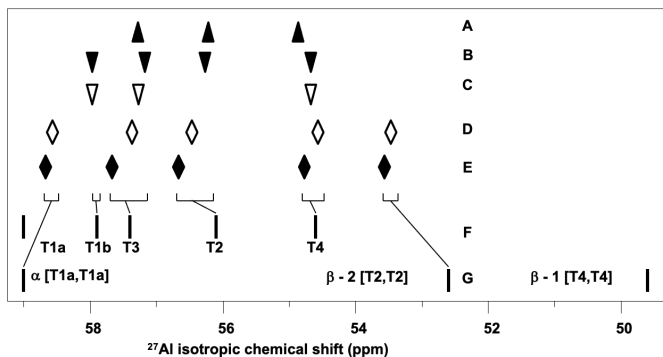
Figure 1. Comparison of the observed (A–E) and calculated (F–G) ^{27}Al isotropic chemical shifts for ferrierites shows the assignment of the ^{27}Al NMR resonances to the T sites. The experimental data for the ferrierites (i) with predominantly isolated single Al: (A) FER/A, (B) FER/B, (C) FER/C and (ii) with isolated single Al as well as Al–O–(Si–O)$_2$–Al sequences: (D) FER/D, (E) FER/E. ^{27}Al isotropic chemical shifts calculated for isolated single Al atoms (F), and for Al–O–(Si–O)$_2$–Al sequences in the α and β cationic sites (G). Adapted Figure 5 from Ref.[27]

18

Our results reveal that the Al siting in the samples with only isolated single Al atoms (A, B, and C) varies with the conditions of the zeolite synthesis. Our results also reveal that the Al siting in ferrierite is not random and depends on the conditions of the zeolite synthesis.

4.6. Effect of Al/Si substitutions and silanol nests on the local geometry of Si and Al framework sites in Si–rich zeolites[30]

^{29}Si and ^{27}Al (3Q) MAS NMR spectroscopy and QM–Pot calculations were employed to investigate the effect of Al/Si substitutions and the presence of silanol nests on the ^{29}Si and ^{27}Al NMR parameters as well as the local geometry of SiO_4 and AlO_4^- tetrahedra of the nearest and next–nearest neighboring Si and Al atoms. The Si–rich zeolite of the chabazite structure (Si/Al 38) was chosen for this study as a representative model of Si–rich zeolites since it exhibits a low number of distinguishable T sites. Our computational results show that an Al/Si substitution causes a downshift of the ^{29}Si chemical shift of the nearest neighboring Si atoms (Al–O–Si) by 4–11 ppm. The effect of a more distant Al/Si substitution (Al–O–Si–O–Si) is significantly less pronounced (downshift up to 2 ppm).

4.7. Formation and local structure of framework Al Lewis sites[38-39]

Employing high resolution ^{27}Al MAS NMR and QM–Pot calculations we show[38] that Al framework (Al_{FR}) Lewis sites formed as minor species created under 300 °C in a zeolite of the FER structure are formed by dehydroxylation of terminal –$(SiO)_3$–AlOH entities tricoordinated to the zeolite framework. The Al_{FR} Lewis sites are reflected in an extremely broad ^{27}Al NMR resonance with $\delta_{iso} \approx 67$ ppm and $C_Q \approx 20$ MHz. Such terminal Al_{FR} Lewis sites are located at internal or external surfaces and are accessible to probe molecules and reactants. We conclude[39] that the observed extremely broad ^{27}Al NMR resonance corresponds to Al_{FR} Lewis sites tricoordinated to the zeolite framework with

adsorbed H_2O. Our calculations yielded δ_{iso} = 59 ppm and C_Q = 16.7 MHz for this site. These theoretical values are in good agreement with the experiment.

Framework Al_{FR} Lewis sites represent a substantial portion of active sites in beta zeolite catalysts activated at low temperatures. We study[39] their nature by ^{27}Al WURST–QCPMG nuclear magnetic resonance (NMR) and propose a plausible mechanism of their formation based on periodic DFT calculations constrained by ^{1}H MAS, ^{27}Al WURST–QCPMG, and ^{29}Si MAS NMR experiments and FTIR measurements. We suggest that these Al_{FR} Lewis sites are formed from Al–OH–Si–O–Si–O–Si–OH–Al sequences located in 12–rings (i.e., close unpaired Al atoms). Our results show that the electron–pair acceptor of Al_{FR} Lewis sites corresponds to an Al_{TRI} atom tricoordinated to the zeolite framework, which adsorbs a water molecule.

4.8. Siting of Li^+ cations as probes in dehydrated zeolites monitored by ^{7}Li MAS NMR spectroscopy[17]

We developed a new method to determine the siting of Li^+ and the local structure of Li^+ sites in crystalline aluminosilicate matrices based on a combination of ^{7}Li–^{7}Li correlation MAS NMR spectroscopy and periodic DFT calculations of the structure of Li^+ sites and subsequent DFT cluster computations of the ^{7}Li NMR shielding. The developed approach can be in general applied to Li^+ cations in other zeolites and various crystalline matrices with large unit cells and a low concentration of Li^+ cations without a significant limitation of their concentration. Our study shows that calculations with an extensive conformational sampling of the cation are required (due to the absence of experimental data regarding the siting of the cation) to obtain the accurate siting of the cation, i.e., employing only optimizations of the structure of the cationic sites in the zeolite framework is not sufficient. Our study of the ferrierite zeolites with isolated single Al atoms (the same three samples as in our prior ^{27}Al (3Q) MAS NMR study[27] were used) reveals that Li^+ cations occupy six distinct cationic sites. Two Li^+ sites are occupied

20

concurrently for Al(T1) and Al(T2) while only one for Al(T3) and Al(T4).

4.9. Siting of Na$^+$ cations as probes in dehydrated zeolites monitored by ^{23}Na (3Q) MAS NMR spectroscopy[21]

We developed a method for the analysis of the siting of monovalent Na$^+$ cations in extra–framework cationic sites in Si–rich ferrierite zeolites. Our study of the ferrierite zeolites with isolated single Al atoms (the same three samples as in our prior ^{27}Al (3Q) MAS NMR study[27] were used) shows that Na$^+$ cations can occupy nine distinct extra–framework cationic sites created by two 6–rings and two 8–rings with one Al atom located in different framework T sites. Eight cationic sites are occupied by Na$^+$ in the three ferrierite samples used. 5–rings do not form cationic sites for Na$^+$ cations. ^{23}Na solid–state NMR spectroscopy can clearly identify the ring accommodating the Na$^+$ cation, while the Al siting in the ring can be determined only for special cases.

4.10. Investigation of the quadrupolar interaction of ^{27}Al nuclei in dehydrated zeolites[19]

We studied the quadrupolar interaction of ^{27}Al nuclei in dehydrated M–forms (M = Li, Na, and K) of chabazite using high–resolution ^{27}Al MAS NMR spectroscopy together with DFT calculations to understand the corresponding high–resolution ^{27}Al MAS NMR spectra. We show that the broadening of the ^{27}Al NMR signal in dehydrated zeolites occurs predominantly because of the deformation of the local structure of AlO$_4^-$ tetrahedra caused by the binding of M$^+$ to the zeolite framework.

4.11. Effects of single and multiple Ge/Si substitutions on the ^{29}Si NMR parameters and the local geometry of SiO$_4$ tetrahedra of the nearest (Ge–O–*Si*) and next–nearest (Ge–O–Si–O–*Si*) neighboring *Si* atoms in zeolites[57]

Employing the zeolite Beta polymorph C (BEC) we examined the effects of one, two, three, and four framework T (T = Ge and Al) atoms as the nearest (T–O–*Si*) neighbors on the ^{29}Si chemical shift and the SiO$_4$ local geometry. Our calculations

reveal a systematic downshift of the ^{29}Si chemical shift of Si by 1–6 ppm and 3–11 ppm for Ge–O–*Si* and Al–O–*Si* sequences, respectively. Furthermore, our results show that the contributions of two, three, and four Ge atoms as the nearest neighbors to the downshift of Si are not additive.

4.12. Structure of Fe(II),[40, 58] Co(II),[15] and Cu(II)[15] cationic sites in ferrierite

Accommodation of Fe(II) cations in the α and β cationic sites of the ferrierite zeolite were investigated using periodic DFT calculations firstly without employing molecular dynamics simulations[58] but subsequently we found that the inclusion of molecular dynamics simulations was required because the binding of bare divalent cations to oxygen atoms of the rings forming cationic sites can lead to significant rearrangements of the local structures of the zeolite framework.[40]

4.13. The organization of Al atoms in the framework Al–rich beta zeolites[18]

Two Al–rich and one Si–rich samples of the beta zeolite were studied by periodic DFT calculations including molecular dynamic simulations together with ^{27}Al and ^{29}Si (CP) MAS NMR, and FTIR of adsorbed acetonitrile–d_3 and UV–vis spectroscopy of Co(II) cations as probes of close Al atoms. Our results show that in contrast to the Si–rich beta zeolites, the Al atoms in the Al–rich beta zeolites are mostly arranged in Al–O–Si–O−Al sequences with their Al atoms facing two different channels, which thus cannot bind bare divalent cations. Only Al atoms in Al–O–$(Si–O)_2$–Al sequences in one ring and a minor fraction of Al–O–Si–O–Al sequences facing the same channel can balance bare divalent cations. The concentration of acid and redox sites in Al–rich beta zeolites, i.e., the potential catalytic active sites, is proportional to the increased Al content in the framework, but without marked change of their structure.

4.14. Al organization and extra–framework sites of bare divalent cations in the TNU−9 zeolite[20]

The aluminum organization in the TUN framework of the TNU–9 zeolite was determined and the locations of the Al pairs forming the corresponding α and β cationic sites for bare divalent cations were suggested. Because the TNU–9 matrix is one of the most complex zeolites known, possessing 24 crystallographically distinguishable framework T sites and a highly complicated channel structure, the standard approach could not have been used. Therefore, we have developed a new significantly improved procedure that includes in addition to the standard methods also ^{27}Al 3Q MAS NMR spectroscopy and extensive periodic DFT calculations, including molecular dynamics. This multi–spectroscopic and theoretical approach was shown to be a very powerful tool for analyzing the siting of aluminum pairs and divalent cations in the TNU–9 zeolite.

4.15. Al organization and extra–framework sites of bare divalent cations in the SSZ–13 zeolite[3]

SSZ–13 is a Si–rich (Si/Al > 5) small pore zeolite of the chabazite topology important for both acid and redox catalysis. The SSZ–13 matrix is not a pentasil–ring zeolite. We developed a new procedure involving ^{27}Al (3Q) MAS NMR spectroscopy and extensive periodic DFT calculations with molecular dynamics, in addition to the standard methods developed for pentasil–ring zeolites based on bare Co(II) cations as probes monitored by FTIR spectroscopy and UV−vis spectroscopy. The location of the Al−O−(Si−O)$_2$−Al and Al−O−(Si−O)$_3$−Al sequences in the zeolite framework was determined (Al−O−Si−O−Al sequences are absent). 54% of the framework Al atoms correspond to Al−O−(Si−O)$_3$−Al sequences which cannot form cationic sites for bare divalent cations but are able to accommodate divalent Co(II) hexaaqua complexes. Employing periodic DFT and ^{27}Al (3Q) MAS NMR spectroscopy we determined that the corresponding Al−O−(Si−O)$_3$−Al sequence is located in two double 6–ring cages with one Al located in the 4–ring connecting two double 6–ring units.

4.16. Modeling of Cu–oxo and Fe–oxo species in the beta zeolite[42]

The periodic DFT calculations including extensive molecular simulations were carried out to model structures whose general spectral features were observed during spectroscopic analysis of Fe and Cu exchanged beta zeolites (one Al–rich and one Si–rich), to obtain more complete information about their possible structures. The calculated dimeric species were coordinated to the framework rings with the known Al distribution in the Al–rich beta zeolite sample determined in our study,[18] which indicated the predominant occurrence of close unpaired Al atoms (66%) linked with an Al−O−(Si−O)$_3$−Al sequence.[3]

4.17. Structure of the distant binuclear Fe(II),[40, 43-44] Co(II),[41, 44] Mn(II)[44] cationic sites in ferrierite

Accommodation of Fe(II), Co(II), and Mn(II) cations in two adjacent β−2 cationic sites of the ferrierite zeolite were investigated using periodic DFT calculations including molecular dynamics simulations. The two adjacent β−2 cationic sites with M(II) form the distant binuclear cationic sites. These computations led to the same rearrangements of the cationic sites upon binding of bare divalent cations to oxygen atoms of the rings forming the cationic sites as in the case of isolated β−2 cationic sites in ferrierite accommodating Fe(II),[40] Co(II),[15] and Cu(II)[15] cations. The optimized structures served for calculations of the formation of the α–oxygen atoms using either N_2O[40-41] or O_2[43-44] molecules.

4.18. Structure of the distant binuclear Fe(II) cationic sites in the beta zeolite[45]

We investigated employing periodic DFT calculations including molecular dynamics simulations the accommodation of Fe(II) cations in two opposite β cationic sites of the beta zeolite. The two opposite β cationic sites are across the 12–ring channel.

4.19. Structure of the distant binuclear Fe(II) cationic sites in mordenite[45]

The binding of Fe(II) cations in two adjacent β cationic sites of mordenite was studied using periodic DFT calculations including molecular dynamics simulations.

5. N₂O decomposition[40, 46, 59]

We used periodic DFT calculations including molecular dynamics together with multiple spectroscopies[40] to study the N₂O decomposition[46] over Fe–ferrierite, Fe–ZSM–5, and Fe–beta zeolite. The results[40] reveal that the distant binuclear Fe(II) sites in Fe–ferrierite are responsible for the superior activity of this catalyst in the N₂O decomposition in the low temperature region. Two Fe(II) cations coordinated in two adjacent β cationic sites of Fe–ferrierite form the active sites for the N₂O decomposition.

The calculated Fe–Fe distance of the active site is 7.4 Å. The formation of the active sites results from a combination of (1) a suitable topology of the ferrierite framework and (2) an appropriate distribution of Al in the distinguishable T sites of the ferrierite framework as well as concentration of Al in these T sites. Both 6–rings forming the two adjacent β cationic sites must contain two Al atoms each (four Al atoms in total).

Our combined experimental and theoretical investigation using an isotope exchange with $N_2^{18}O$ revealed that zeolite–framework O atoms were involved in the formation of O_2 molecules during the N₂O decomposition catalyzed by Fe–ferrierite. We suggested plausible mechanisms of the isotope exchange.[59]

6. Formation of the α−oxygen atom on the distant binuclear Co(II) sites in Co–ferrierite from N_2O[41]

Our study reveals for the first time that the α−oxygen with notable oxidation properties can be prepared not only on a Fe(II)−zeolite but also on a zeolite exchanged with two other divalent cations: Co(II) and Ni(II). The variability of the type of the cation forming the distant binuclear active sites can potentially allow the tuning of the corresponding catalytic

properties. The α−oxygen is formed over all the three M(II)−ferrierite samples (M = Co(II), Ni(II), and Fe(II)) by the abstraction of the oxygen atom from N_2O by the distant binuclear M(II) sites. The M(II) cations are accommodated in two adjacent β−2 cationic sites of M(II)−ferrierite and create the distant binuclear active sites responsible for the formation of the α−oxygen. The α−oxygen is then able to selectively oxidize methane mainly to methanol at room temperature. Only the distant binuclear Co(II)...Co(II) structures and not isolated Co(II) cations are active in the formation of the α−oxygen while both the types of Fe(II) cations are potent to yield the α−oxygen.

N_2O adsorbs by the N terminal atom on one Co(II) cation. The O atom of the adsorbed N_2O is well positioned to oxidize the other Co(II) cation to yield the α−oxygen and adsorbed N_2 after the N−O bond cleavage. The calculated barrier is 25.0 kcal/mol. This value indicates that the oxidation of Co(II) to give the α−oxygen should be facile but significantly more sluggish than the same reaction step on Fe(II)−ferrierite (i.e., the barrier of 14.5 kcal/mol).

7. Splitting dioxygen at room temperature to form the active α−oxygen for methane oxidation at room temperature[43]

Activation of dioxygen is a basic enzymatic reaction of living organism while mimicking this process over artificial inorganic systems represents a great challenge. The activation of dioxygen gained significance as a possible key for the usage of methane. Methane as the main component of natural gas became abundant because of the development of the shale gas technology. Nevertheless, until now, productions of energy (electricity and heat) and hydrogen represent the main utilization of the methane production. Therefore, the transformation of methane to liquid products representing energy carriers and chemical production platforms is in high demand. The selective oxidation of methane to methanol is suggested to be an encouraging way of a methane−to−liquid transformation. However, only the selective oxidation of methane by dioxygen is economically feasible and represents

a promising system of the utilization of methane with an enormous industrial impact.

7.1. The role of distant binuclear M(II) sites in M−ferrierite[40-41, 43-44, 53]

Our studies showed that M(II) (M = Co(II), Ni(II), and Fe(II)) cations exchanged in the ferrierite zeolite form distant binuclear cationic structures which significantly facilitate the abstraction of the oxygen atom from N_2O to yield the highly active α−oxygen on the M(II) cation. The M(II) cations forming these species are located in two adjacent extra−framework cationic β sites. The calculated distance of the two M(II) cations is ca. 7.4 Å. In contrast to isolated M(II) cations, the binuclear M(II) species can arrange a four−electron reaction. These distant binuclear M(II) sites in M(II)−ferrierite exhibit a resemblance in geometry and the oxidation state with iron active sites of methane monooxygenases; however, the distance between the two Fe cations in the enzymes is less than half of that in M(II)−ferrierite. This raised a question if distant binuclear M(II) structures were able to cleave dioxygen and form a pair of the distant α−oxygen atoms on the two M cations which afterward can oxidize methane to methanol. Employing periodic DFT calculations in tandem with Mössbauer (only for Fe) and FTIR spectroscopies and stoichiometric reaction tests we answered this question.

7.2. Splitting dioxygen over Fe(II)−ferrierite[43]

Our periodic DFT calculations of Fe(II)−ferrierite reveal that two Fe(II) cations forming distant binuclear cationic structures can indeed cleave dioxygen to form two α−oxygen atoms.

Figure 2 shows the calculated mechanism of the cleavage. An $O_2(g)$ molecule that is in a triplet state adsorbs on one of the Fe(II) cations to yield a [Fe OOmono...Fe]′ monodentate complex **2′** with the O_2 moiety in a triplet state. **2′** either undergoes a spin crossover to give a [Fe OOmono...Fe] monodentate complex **2**, which has the O_2 moiety in a singlet state, or rearranges its structure to form a

[Fe OObi...Fe]′ bidentate complex **3′**. In the latter case, a spin change occurs and a [Fe OObi...Fe] bidentate complex **3** with the O_2 moiety in a singlet state is yielded. The oxidation occurs from the most stable bidentate complex **3**, which rearranges to the less stable monodentate complex **2**. The adsorbed O_2 moiety of **2** is better positioned for the interaction with the other Fe(II) located in the adjacent β site. Subsequently, dioxygen is cleaved via a [Fe−O−O−Fe] transition state **TS** to yield a [Fe═O O═Fe] complex **4** in a concerted manner. Both Fe in **4** are oxidized to form a pair of the distant α−oxygen atoms. The reaction energy of the reaction from 1 + O_2(g) to give **4** is −24.7 kcal/mol. The calculated barrier of the cleavage of dioxygen is 24.9 kcal/mol, indicating that the oxidation should be facile but substantially more sluggish than the oxidation of the same Fe(II)−ferrierite by N_2O (i.e., the barrier of 14.5 kcal/mol[41]).
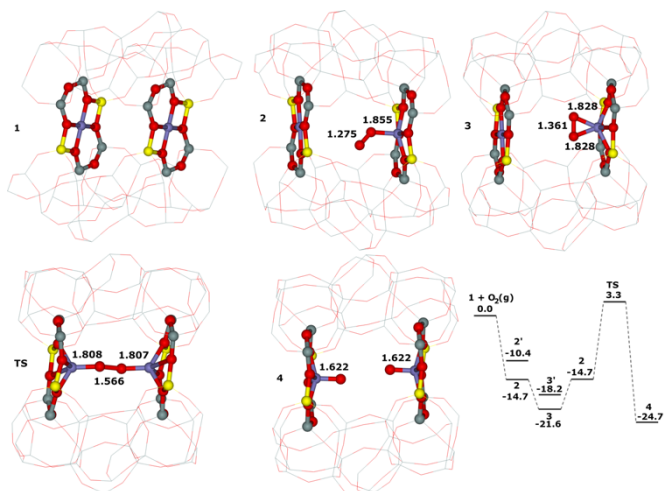
Figure 2. Optimized structures of the two adjacent β sites of Fe−ferrierite **1** after molecular dynamics simulations (top, left), the monodentate [Fe OOmono…Fe] complex **2** formed in the two adjacent β sites (top, middle), the bidentate [Fe OObi…Fe] complex **3** formed in the two adjacent β sites (top,

28

right), the [Fe−O−O−Fe] transition state **TS** created in the two adjacent β sites (bottom, left), the [Fe≡O O≡Fe] product **4** created in the two adjacent β sites (bottom, middle). The distances are in Å. Silicon atoms are in gray, oxygen atoms in red, aluminum atoms in yellow, and iron atoms in blue. Schematic energy profile (in kcal mol-1) of the formation of the [Fe≡O O≡Fe] product (bottom, right). Adapted Figure 1 from Ref.[43]

Our Mössbauer and FTIR experiments and stoichiometric reaction tests show that methane can be oxidized by dioxygen over distant binuclear Fe(II) species stabilized in an aluminosilicate matrix. Both the formation of the α−oxygen atoms and the oxidation of methane to methanol occur at room temperature. This outcome indicates a breakthrough in the development of the technology of the transformation of methane to liquid products representing energy carriers and chemical production platforms. Nevertheless, the application in the chemical industry requires a further development of a long−term stable system with a high activity in the methane conversion.

7.3. Splitting dioxygen over M(II)−ferrierite (M = Co(II) and Mn(II))[44, 53]
Our periodic DFT computations for Co(II)−ferrierite and Mn(II)−ferrierite reveal that our breakthrough in the activation of dioxygen is not limited exclusively to Fe(II) cations but the ability of dioxygen splitting represents a general property of the distant binuclear M(II) centers capable of the M(II) to M(IV) redox cycle with the M...M distance of ca 7.4 Å stabilized in M−ferrierite. Our results reveal that the distant binuclear M(II) (M(II) = Co(II) and Mn(II)) sites located in two adjacent β sites of ferrierite can split dioxygen and form a pair of the α–oxygen species which were reported to be very active in the oxidation of methane to methanol.

The calculated mechanisms of splitting dioxygen for Co(II)–ferrierite and Mn(II)–ferrierite are generally the same as that for Fe(II)–ferrierite. The calculated barrier of 24.3 kcal/mol for Co(II)–ferrierite is essentially the same as that

for Fe(II)–ferrierite (24.9 kcal/mol) while the barrier for Mn(II)–ferrierite is significantly higher (36.8 kcal/mol) indicating that the cleavage of dioxygen over Mn(II)–ferrierite is expected to be more sluggish.

Our FTIR experiments and stoichiometric reaction tests confirmed the creation of a pair of the α–oxygen species for Co(II)–ferrierite, Mn(II)–ferrierite, and Ni(II)–ferrierite at room temperature and the subsequent oxidation of methane to methanol at room temperature as well.

7.4. Splitting dioxygen over Fe(II)−zeolites other than ferrierite[45]

The effects of the local arrangement of distant binuclear Fe(II) centers and framework topology on the ability to split dioxygen to form a pair of the α–oxygen atoms was investigated in a subsequent study. The goal of the study was to answer a question whether the low barriers of the cleavage of dioxygen result from the unique topology of the ferrierite zeolite and the Al organization (especially the Al siting in the rings forming the cationic sites) in the ferrierite used or if the activity regarding splitting dioxygen represents a general property of the distant binuclear Fe(II) centers stabilized in the aluminosilicate matrix. If the latter is true, it can represent a highly promising base for the development of exceptionally active systems with higher concentrations of the active sites for the direct oxidation of methane. Moreover, splitting dioxygen over the distant binuclear Fe(II) centers located at the opposite sides of the wall of larger channels potentially opens the possibility of using the α–oxygen atoms also for the direct oxidation of bulkier molecules with a restricted access to the α–oxygen atoms through 8–rings (i.e., via the ferrierite side channel).

Our results reveal that the distant binuclear Fe(II) sites with suitable parameters accommodated in various zeolites can split dioxygen and form a pair of the α–oxygen atoms able to oxidize methane to methanol. Therefore, the ability to cleave dioxygen represents a general property of the distant binuclear Fe(II) centers stabilized in aluminosilicate matrices, thus suggesting the possibility of developing Fe–

zeolite–based systems for the dioxygen activation for direct oxidations using various zeolite matrices. The suitable parameters are found to be the two cationic sites forming the distant binuclear Fe(II) centers have to (i) face each other, (ii) be parallel, and (iii) be axial. (iv) The Fe···Fe distance has to lie in a narrow range from ca. 7 to ca. 8 Å (ca. 7−ca. 10 Å for the distance between the two rings (forming the corresponding cationic sites) in empty zeolites since this distance is equal or larger than the Fe···Fe distances).

7.5. Splitting dioxygen over M(II)−zeolites

Based on our studies of M(II)–ferrierite[43-44, 53] (M(II) = Fe(II), Co(II), Mn(II) and Ni(II)) and Fe(II)–zeolite[45] (zeolite = ferrierite, mordenite, beta, and A zeolites) we can generalize that the distant binuclear M(II) centers capable of the M(II) to M(IV) redox cycle and with the suitable parameters can cleave dioxygen to form a pair of the α–oxygen atoms able to oxidize methane to methanol. This suggests the possibility of developing M(II)–zeolite based tunable systems for the activation of dioxygen for direct oxidations using various transition metal cations in various zeolite matrices.

7.6. Reactivity of the distant binuclear Fe(II) centers[54]

We used periodic DFT calculations to investigate the detailed mechanism of the reduction of Fe(IV)=O of Fe–ferrierite by dihydrogen. The findings attained for the Fe(IV)=O centers of pairs of the distant α–oxygen atoms were compared with those obtained for the isolated Fe(IV)=O sites. The oxidation of dihydrogen, which is the simplest oxidation reaction, was chosen for comparison of the activity of both the types of Fe(IV)=O.

The obtained results clearly evidence (and most likely can be generalized for other molecules than dihydrogen as well) that the proximity of the other Fe(IV)=O site in the confined reaction space of the zeolite cavity can dramatically change the behavior of both the cooperating α–oxygen atoms and the reaction mechanism over Fe(IV)=O sites of a pair of the distant α–oxygen atoms can differ from that over isolated Fe(IV)=O sites.

8. Conclusions

Our work significantly contributed to the determination of the organization of Al atoms in the framework of industrially important Si–rich zeolite catalysts. The Al organization is a key property and its knowledge is required to evaluate the potential of a zeolite for individual catalytic reactions.

Our development of the bare zeolite framework model permitted the employment of realistic models for our DFT calculations of the local geometry of AlO_4^- tetrahedra in fully hydrated, cation–containing silicon–rich zeolites, and subsequently the evaluation of ^{27}Al isotropic chemical shifts which allowed for the first time the partial determination of the Al siting for the ZSM–5 zeolite and the full resolution of the Al siting for the ferrierite zeolite. We showed that the Al siting is neither random nor controlled by a simple rule but it depends on the conditions of the zeolite synthesis. Our achievements clearly demonstrate the power of the high–resolution ^{27}Al MAS NMR experiment combined with DFT calculations and also support the bare zeolite framework model adopted in our calculations.

We developed a method which uses periodic DFT calculations and ^7Li and ^{23}Na MAS NMR experiments for the analysis of the siting of monovalent Li^+ and Na^+, respectively, cations in extra–framework cationic sites in Si–rich ferrierite zeolites. These monovalent cations in dehydrated zeolite frameworks can be used as additional probes of the Al organization. Li^+ cations as probes can determine the Al siting while Na^+ cations as probes can clearly identify the ring accommodating the Na^+ cation, while the Al siting in that ring can be determined only for special cases. Our studies of the siting of monovalent Li^+ and Na^+ are the first ones which determine the local structure of Li^+ and Na^+, respectively, extra–framework cationic sites in a Si–rich zeolite with no knowledge of the Li^+ and Na^+, respectively, cationic sites from diffraction experiments.

Employing ^{27}Al solid–state NMR and FTIR experiments in tandem with DFT calculations we determined for the first time that framework Al Lewis sites correspond to Al atoms tricoordinated to the zeolite framework, and furthermore, we suggested a plausible mechanism of their formation in the beta zeolite.

Using only the power of DFT calculations we determined the local structure of cationic sites for bare divalent transition metal cations (i.e., Fe(II), Co(II), Mn(II), and Cu(II)) and showed that these cations upon binding to cationic sites induced a rearrangement of the local structure of the zeolite framework. The local structure of cationic sites for bare divalent transition metal cations cannot be determined by diffraction methods.

The knowledge of (i) the organization of Al atoms in the framework of Si–rich zeolites and (ii) the local structure of cationic sites for bare divalent transition metal cations in these zeolites was a necessary condition of our (i) identification of the distant binuclear cationic sites and (ii) theoretical prediction of their ability to split dioxygen afterward confirmed by experiments.

We recognized the distant binuclear cationic sites using only theoretical modeling of the N_2O decomposition over Fe–zeolites. The distant binuclear Fe(II) sites are responsible for the superior activity of Fe–ferrierite in the N_2O decomposition in the low temperature region. Afterward, we predicted using solely the power of periodic DFT calculations that these distant binuclear Fe(II) sites were able to split dioxygen to yield pairs of the distant α–oxygen atoms able to oxidize methane to methanol at room temperature. This theoretical prediction was subsequently confirmed by experiments and thus splitting dioxygen was discovered. This achievement represents a breakthrough in oxidation catalysis.

Theoretical modeling further clearly showed that this breakthrough in the activation of dioxygen was not limited exclusively to Fe(II) cations and the structure of the ferrierite zeolite. The ability of dioxygen splitting represents a general property of the distant binuclear M(II) centers accommodated in a zeolite matrix if the M(II) cations (i) are capable of the M(II) to M(IV) redox cycle and (ii) have suitable structural parameters. Our achievements open the possibility of developing highly active and selective systems employed for the direct oxidation of (i) methane to methanol and (ii) other organic compounds to valuable oxidation products.

References

(1) Catlow, C. R.; Davidson, M.; Hardacre, C.; Hutchings, G. J. *Philos. Trans. R. Soc. A* **2016**, *374*, 20150089.

(2) Sklenak, S.; Dedecek, J.; Li, C. B.; Wichterlova, B.; Gabova, V.; Sierka, M.; Sauer, J. *Angew. Chem., Int. Ed.* **2007**, *46*, 7286-7289.

(3) Mlekodaj, K.; Dedecek, J.; Pashkova, V.; Tabor, E.; Klein, P.; Urbanova, M.; Karcz, R.; Sazama, P.; Whittleton, S. R.; Thomas, H. M.; Fishchuk, A. V.; Sklenak, S. *J. Phys. Chem. C* **2019**, *123*, 7968-7987.

(4) Dedecek, J.; Sobalik, Z.; Wichterlova, B. *Catal. Rev. Sci. Eng.* **2012**, *54*, 135-223.

(5) Dedecek, J.; Tabor, E.; Sklenak, S. *ChemSusChem* **2019**, *12*, 556-576.

(6) Knott, B. C.; Nimlos, C. T.; Robichaud, D. J.; Nimlos, M. R.; Kim, S.; Gounder, R. *ACS Catal.* **2018**, *8*, 770-784.

(7) Baerlocher, C.; McCusker, L. B. Database of Zeolite Structures: http://www.iza-structure.org/databases/ (accessed April 25, 2022).

(8) Pashkova, V.; Sklenak, S.; Klein, P.; Urbanova, M.; Dedecek, J. *Chem. Eur. J.* **2016**, *22*, 3937-3941.

(9) Dedecek, J.; Wichterlova, B. *J. Phys. Chem. B* **1999**, *103*, 1462-1476.

(10) Kaucky, D.; Dedecek, J. I.; Wichterlova, B. *Microporous Mesoporous Mater.* **1999**, *31*, 75-87.

(11) Dedecek, J.; Kaucky, D.; Wichterlova, B. *Microporous Mesoporous Mater.* **2000**, *35-6*, 483-494.

(12) Dedecek, J.; Kaucky, D.; Wichterlova, B. *Chem. Commun.* **2001**, 970-971.

(13) Dedecek, J.; Kaucky, D.; Wichterlova, B.; Gonsiorova, O. *Phys. Chem. Chem. Phys.* **2002**, *4*, 5406-5413.

(14) Gabova, V.; Dedecek, J.; Cejka, J. *Chem. Commun.* **2003**, 1196-1197.

(15) Sklenak, S.; Andrikopoulos, P. C.; Whittleton, S. R.; Jirglova, H.; Sazama, P.; Benco, L.; Bucko, T.; Hafner, J.; Sobalik, Z. *J. Phys. Chem. C* **2013**, *117*, 3958-3968.

(16) Sobalik, Z.; Sazama, P.; Dedecek, J.; Wichterlova, B. *Appl. Catal., A* **2014**, *474*, 178-185.

(17) Klein, P.; Dedecek, J.; Thomas, H. M.; Whittleton, S. R.; Pashkova, V.; Brus, J.; Kobera, L.; Sklenak, S. *Chem. Commun.* **2015**, *51*, 8962-8965.

(18) Sazama, P.; Tabor, E.; Klein, P.; Wichterlova, B.; Sklenak, S.; Mokrzycki, L.; Pashkkova, V.; Ogura, M.; Dedecek, J. *J. Catal.* **2016**, *333*, 102-114.

(19) Klein, P.; Pashkova, V.; Thomas, H. M.; Whittleton, S. R.; Brus, J.; Kobera, L.; Dedecek, J.; Sklenak, S. *J. Phys. Chem. C* **2016**, *120*, 14216-14225.

(20) Karcz, R.; Dedecek, J.; Supronowicz, B.; Thomas, H. M.; Klein, P.; Tabor, E.; Sazama, P.; Pashkova, V.; Sklenak, S. *Chem. Eur. J.* **2017**, *23*, 8857-8870.

(21) Klein, P.; Dedecek, J.; Thomas, H. M.; Whittleton, S. R.; Klimes, J.; Brus, J.; Kobera, L.; Bryce, D. L.; Sklenak, S. *J. Phys. Chem. C* **2022**, *126*, 10686-10702.

(22) Dedecek, J.; Wichterlova, B. *Phys. Chem. Chem. Phys.* **1999**, *1*, 629-637.

(23) Dedecek, J.; Capek, L.; Wichterlova, B. *Appl. Catal., A* **2006**, *307*, 156-164.

(24) Zhang, L. W.; Zhang, H. K.; Chen, Z. Q.; Ning, Q.; Liu, S. Y.; Ren, J.; Wen, X. D.; Li, Y. W. *Catal. Sci. Technol.* **2019**, *9*, 7034-7044.

(25) Wang, S.; He, Y.; Jiao, W. Y.; Wang, J. G.; Fan, W. B. *Curr. Opin. Chem. Eng.* **2019**, *23*, 146-154.

(26) Sklenak, S.; Dedecek, J.; Li, C.; Wichterlova, B.; Gabova, V.; Sierka, M.; Sauer, J. *Phys. Chem. Chem. Phys.* **2009**, *11*, 1237-1247.

(27) Dedecek, J.; Lucero, M. J.; Li, C. B.; Gao, F.; Klein, P.; Urbanova, M.; Tvaruzkova, Z.; Sazama, P.; Sklenak, S. *J. Phys. Chem. C* **2011**, *115*, 11056-11064.

(28) Sklenak, S.; Dedecek, J.; Li, C. B.; Gao, F.; Jansang, B.; Boekfa, B.; Wichterlova, B.; Sauer, J. *Collect. Czech. Chem. Commun.* **2008**, *73*, 909-920.

(29) Dedecek, J.; Sklenak, S.; Li, C.; Wichterlova, B.; Gabova, V.; Brus, J.; Sierka, M.; Sauer, J. *J. Phys. Chem. C* **2009**, *113*, 1447-1458.

(30) Dedecek, J.; Sklenak, S.; Li, C. B.; Gao, F.; Brus, J.; Zhu, Q. J.; Tatsumi, T. *J. Phys. Chem. C* **2009**, *113*, 14454-14466.

(31) Vjunov, A.; Fulton, J. L.; Huthwelker, T.; Pin, S.; Mei, D.; Schenter, G. K.; Govind, N.; Camaioni, D. M.; Hu, J. Z.; Lercher, J. A. *J. Am. Chem. Soc.* **2014**, *136*, 8296-8306.

(32) Holzinger, J.; Nielsen, M.; Beato, P.; Brogaard, R. Y.; Buono, C.; Dyballa, M.; Falsig, H.; Skibsted, J.; Svelle, S. *J. Phys. Chem. C* **2019**, *123*, 7831-7844.

(33) Kiricsi, I.; Flego, C.; Pazzuconi, G.; Parker, W. O.; Millini, R.; Perego, C.; Bellussi, G. *J. Phys. Chem.* **1994**, *98*, 4627-4634.

(34) Corma, A.; Garcia, H. *Chem. Rev.* **2002**, *102*, 3837-3892.

(35) Cejka, J.; Wichterlova, B. *Catal. Rev. Sci. Eng.* **2002**, *44*, 375-421.

(36) Corma, A. *Chem. Rev.* **1995**, *95*, 559-614.

(37) van Bokhoven, J. A.; van der Eerden, A. M. J.; Koningsberger, D. C. *J. Am. Chem. Soc.* **2003**, *125*, 7435-7442.

(38) Brus, J.; Kobera, L.; Schoefberger, W.; Urbanova, M.; Klein, P.; Sazama, P.; Tabor, E.; Sklenak, S.; Fishchuk, A. V.; Dedecek, J. *Angew. Chem., Int. Ed.* **2015**, *54*, 541-545.

(39) Kobera, L.; Dedecek, J.; Klein, P.; Tabor, E.; Brus, J.; Fishchuk, A. V.; Sklenak, S. *J. Chem. Phys.* **2022**, *156*, 104702.

(40) Sklenak, S.; Andrikopoulos, P. C.; Boekfa, B.; Jansang, B.; Novakova, J.; Benco, L.; Bucko, T.; Hafner, J.; Dedecek, J.; Sobalik, Z. *J. Catal.* **2010**, *272*, 262-274.

(41) Tabor, E.; Lemishka, M.; Sobalik, Z.; Mlekodaj, K.; Andrikopoulos, P. C.; Dedecek, J.; Sklenak, S. *Commun. Chem.* **2019**, *2*, 71.

(42) Sazama, P.; Moravkova, J.; Sklenak, S.; Vondrov, A.; Tabor, E.; Sadovska, G.; Pilar, R. *ACS Catal.* **2020**, *10*, 3984-4002.

(43) Tabor, E.; Dedecek, J.; Mlekodaj, K.; Sobalik, Z.; Andrikopoulos, P. C.; Sklenak, S. *Sci. Adv.* **2020**, *6*, eaaz9776.

(44) Dedecek, J.; Tabor, E.; Andrikopoulos, P. C.; Sklenak, S. *Int. J. Quantum Chem.* **2021**, *121*, e26611.

(45) Tabor, E.; Lemishka, M.; Olszowka, J. E.; Mlekodaj, K.; Dedecek, J.; Andrikopoulos, P. C.; Sklenak, S. *ACS Catal.* **2021**, *11*, 2340-2355.

(46) Jisa, K.; Novakova, J.; Schwarze, M.; Vondrova, A.; Sklenak, S.; Sobalik, Z. *J. Catal.* **2009**, *262*, 27-34.

(47) Panov, G. I.; Sobolev, V. I.; Kharitonov, A. S. *J. Mol. Catal.* **1990**, *61*, 85-97.

(48) Panov, G. I.; Kharitonov, A. S.; Sobolev, V. I. *Appl. Catal., A* **1993**, *98*, 1-20.

(49) Sobolev, V. I.; Dubkov, K. A.; Panna, O. V.; Panov, G. I. *Catal. Today* **1995**, *24*, 251-252.

(50) Dubkov, K. A.; Sobolev, V. I.; Talsi, E. P.; Rodkin, M. A.; Watkins, N. H.; Shteinman, A. A.; Panov, G. I. *J. Mol. Catal., A* **1997**, *123*, 155-161.

(51) Dubkov, K. A.; Ovanesyan, N. S.; Shteinman, A. A.; Starokon, E. V.; Panov, G. I. *J. Catal.* **2002**, *207*, 341-352.

(52) Yuan, S.; Li, Y. D.; Peng, J. Y.; Questell-Santiago, Y. M.; Akkiraju, K.; Giordano, L.; Zheng, D. J.; Bagi, S.; Roman-Leshkov, Y.; Shao-Horn, Y. *Adv. Energy Mater.* **2020**, *10*, 2002154.

(53) Mlekodaj, K.; Lemishka, M.; Sklenak, S.; Dedecek, J.; Tabor, E. *Chem. Commun.* **2021**, *57*, 3472-3475.

(54) Sklenak, S.; Groizard, T.; Jirglova, H.; Sazama, P.; Dedecek, J. *J. Phys. Chem. C* **2022**, *126*, 4854-4861.

(55) Adiga, S.; Aebi, D.; Bryce, D. L. *Can. J. Chem.* **2007**, *85*, 496-505.

(56) Mortier, W. J. *Zeolites* **1982**, *38*, 1-67.

(57) Whittleton, S. R.; Vicente, A.; Fernandez, C.; Rastegar, S. F.; Fishchuk, A. V.; Sklenak, S. *Microporous Mesoporous Mater.* **2018**, *267*, 124-133.

(58) Benco, L.; Bucko, T.; Grybos, R.; Hafner, J.; Sobalik, Z.; Dedecek, J.; Sklenak, S.; Hrusak, J. *J. Phys. Chem. C* **2007**, *111*, 9393-9402.

(59) Andrikopoulos, P. C.; Sobalik, Z.; Novakova, J.; Sazama, P.; Sklenak, S. *ChemPhysChem* **2013**, *14*, 520-531.

Publications used in this thesis

1. Lubomir Benco, Tomas Bucko, Robert Grybos, Juergen Hafner, Zdenek Sobalik, Jiri Dedecek, Stepan Sklenak, and J. Hrusak *J. Phys. Chem. C*, **2007**, *111*, 9393-9402.
2. Stepan Sklenak, Jiri Dedecek, Chengbin Li, Blanka Wichterlova, Vendula Gabova, Marek Sierka and Joachim Sauer *Angew. Chem., Int. Ed.*, **2007**, *46*, 7286-7289.
3. Stepan Sklenak, Jiri Dedecek, Chengbin Li, Fei Gao, Bavornpon Jansang, Bundet Boekfa, Blanka Wichterlova, and Joachim Sauer *Collect. Czech. Chem. Commun.*, **2008**, *73*, 909-920.
4. Stepan Sklenak, Jiri Dedecek, Chengbin Li, Blanka Wichterlova, Vendula Gabova, Marek Sierka, and Joachim Sauer *Phys. Chem. Chem. Phys.*, **2009**, *11*, 1237-1247.
5. Jiri Dedecek, Stepan Sklenak, Chengbin Li, Blanka Wichterlova, Vendula Gabova, Jiri Brus, Marek Sierka, and Joachim Sauer *J. Phys. Chem. C*, **2009**, *113*, 1447-1458.
6. Kamil Jisa, Jana Novakova, Michal Schwarze, Alena Vondrova, Stepan Sklenak, and Zdenek Sobalik *J. Catal.*, **2009**, *262*, 27-34.
7. Jiri Dedecek, Stepan Sklenak, Chengbin Li, Fei Gao, Jiri Brus, Qingjun Zhu, and Takashi Tatsumi *J. Phys. Chem. C*, **2009**, *113*, 14454-14466.
8. Stepan Sklenak, Prokopis C. Andrikopoulos, Bundet Boekfa, Bavornpon Jansang, Jana Novakova, Lubomir Benco, Tomas Bucko, Juergen Hafner, Jiri Dedecek, and Zdenek Sobalik *J. Catal.*, **2010**, *272*, 262-274.
9. Jiri Dedecek, Melissa J. Lucero, Chengbin Li, Fei Gao, Petr Klein, Martina Urbanova, Zdenka Tvaruzkova, Petr Sazama, and Stepan Sklenak *J. Phys. Chem. C*, **2011**, *115*, 11056-11064.
10. Prokopis C. Andrikopoulos, Zdenek Sobalik, Jana Novakova, Petr Sazama, Stepan Sklenak *ChemPhysChem*, **2013**, *14*, 520-531.
11. Stepan Sklenak, Prokopis C. Andrikopoulos, Sarah R. Whittleton, Hana Jirglova, Petr Sazama, Lubomir Benco, Tomas Bucko, Juergen Hafner, and Zdenek Sobalik *J. Phys. Chem. C*, **2013**, *117*, 3958-3968.

12. Jiri Brus, Libor Kobera, Wolfgang Schoefberger, Martina Urbanova, Petr Klein, Petr Sazama, Edyta Tabor, Stepan Sklenak, Anna V. Fishchuk, and Jiri Dedecek *Angew. Chem., Int. Ed.*, **2015**, *54*, 541-545.

13. Petr Klein, Jiri Dedecek, Haunani M. Thomas, Sarah R. Whittleton, Veronika Pashkova, Jiri Brus, Libor Kobera, and Stepan Sklenak *Chem. Commun.*, **2015**, *51*, 8962-8965.

14. Petr Sazama, Edyta Tabor, Petr Klein, Blanka Wichterlova, Stepan Sklenak, Lukas Mokrzycki, Veronika Pashkkova, Masaru Ogura, Jiri Dedecek *J. Catal.*, **2016**, *333*, 102-114.

15. Veronika Pashkova, Stepan Sklenak, Petr Klein, Martina Urbanova, and Jiri Dedecek *Chem. Eur. J.*, **2016**, *22*, 3937-3941.

16. Petr Klein, Veronika Pashkova, Haunani M. Thomas, Sarah R. Whittleton, Jiri Brus, Libor Kobera, Jiri Dedecek, and Stepan Sklenak *J. Phys. Chem. C*, **2016**, *120*, 14216-14225.

17. Robert Karcz, Jiri Dedecek, Barbara Supronowicz, Haunani M. Thomas, Petr Klein, Edyta Tabor, Petr Sazama, Veronika Pashkova, and Stepan Sklenak *Chem. Eur. J.*, **2017**, *23*, 8857-8870.

18. Sarah R. Whittleton, Aurelie Vicente, Christian Fernandez, Somayeh F. Rastegar, Anna V. Fishchuk, Stepan Sklenak *Microporous Mesoporous Mater.*, **2018**, *267*, 124-133.

19. Kinga Mlekodaj, Jiri Dedecek, Veronika Pashkova, Edyta Tabor, Petr Klein, Martina Urbanova, Robert Karcz, Petr Sazama, Sarah R. Whittleton, Haunani M. Thomas, Anna V. Fishchuk, and Stepan Sklenak *J. Phys. Chem. C*, **2019**, *123*, 7968-7987.

20. Jiri Dedecek, Edyta Tabor, and Stepan Sklenak *ChemSusChem*, **2019**, *12*, 556-576.

21. Edyta Tabor, Mariia Lemishka, Zdenek Sobalik, Kinga Mlekodaj, Prokopis C. Andrikopoulos, Jiri Dedecek, Stepan Sklenak *Commun. Chem.*, **2019**, *2*: 71.

22. Petr Sazama, Jaroslava Moravkova, Stepan Sklenak, Alena Vondrova, Edyta Tabor, Galina Sadovska, and Radim Pilar *ACS Catal.*, **2020**, *10*, 3984-4002.

23. Edyta Tabor, Jiri Dedecek, Kinga Mlekodaj, Zdenek Sobalik, Prokopis C. Andrikopoulos, Stepan Sklenak *Sci. Adv.*, **2020**, *6*: eaaz9776.

24. Jiri Dedecek, Edyta Tabor, Prokopis C. Andrikopoulos, Stepan Sklenak *Int. J. Quantum. Chem.,* **2021**, *121*, e26611.

25. Edyta Tabor, Mariia Lemishka, Joanna E. Olszowka, Kinga Mlekodaj, Jiri Dedecek, Prokopis C. Andrikopoulos, and Stepan Sklenak *ACS Catal.,* **2021**, *11*, 2340-2355.

26. Kinga Mlekodaj, Mariia Lemishka, Stepan Sklenak, Jiri Dedecek, and Edyta Tabor *Chem. Commun.*, **2021**, *57*, 3472–3475.

27. Libor Kobera, Jiri Dedecek, Petr Klein, Edyta Tabor, Jiri Brus, Anna V. Fishchuk, and Stepan Sklenak *J. Chem. Phys.*, **2022**, *156*, 104702.

28. Stepan Sklenak, Thomas Groizard, Hana Jirglova, Petr Sazama, and Jiri Dedecek *J. Phys. Chem. C*, **2022**, *126*, 4854-4861.

29. Petr Klein, Jiri Dedecek, Haunani M. Thomas, Sarah R. Whittleton, Jiri Klimes, Jiri Brus, Libor Kobera, David L. Bryce, and Stepan Sklenak *J. Phys. Chem. C*, **2022**, *126*, 10686-10702.